analytical chemistry

Technical Note

pubs.acs.org/ac

Tissue Characterization with Quantitative High-Resolution Magic Angle Spinning Chemical Exchange Saturation Transfer Z-Spectroscopy

Iris Yuwen Zhou,[†] Taylor L. Fuss,[†,‡] Takahiro Igarashi,[†,§] Weiping Jiang,[†,∥] Xin Zhou,[∥] Leo L. Cheng,[†,‡] and Phillip Zhe Sun*[,†]

[†]Athinoula A. Martinos Center for Biomedical Imaging, Department of Radiology, Massachusetts General Hospital and Harvard Medical School, Charlestown, Massachusetts 02129, United States

[‡]Department of Pathology, Massachusetts General Hospital and Harvard Medical School, Boston, Massachusetts 02114, United States

[§]Division of Neurosurgery, Department of Neurological Surgery, Nihon University School of Medicine, Tokyo 173-8610, Japan

[∥]State Key Laboratory of Magnetic Resonance and Atomic and Molecular Physics, National Center for Magnetic Resonance in Wuhan, Wuhan Institute of Physics and Mathematics, Chinese Academy of Sciences, Wuhan 430071, China

Supporting Information

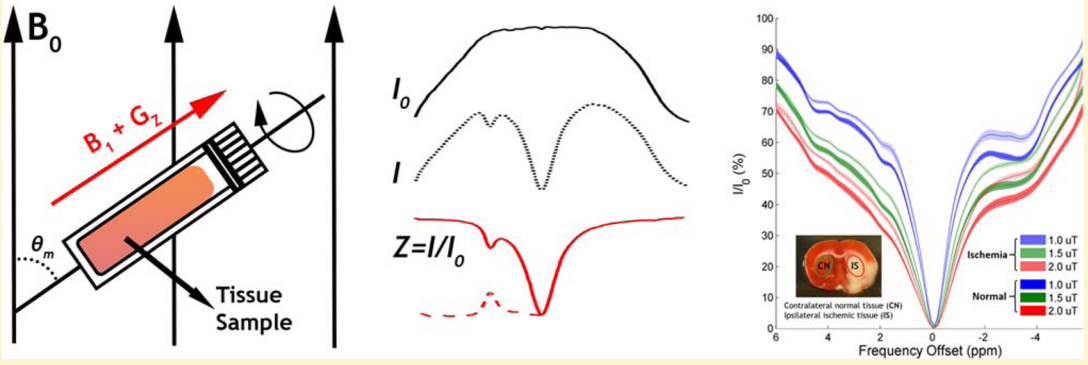

ABSTRACT: Chemical exchange saturation transfer (CEST) provides sensitive magnetic resonance (MR) contrast for probing dilute compounds via exchangeable protons, serving as an emerging molecular imaging methodology. CEST Z-spectrum is often acquired by sweeping radiofrequency saturation around bulk water resonance, offset by offset, to detect CEST effects at characteristic chemical shift offsets, which requires prolonged acquisition time. Herein, combining high-resolution magic angle spinning (HRMAS) with concurrent application of gradient and rf saturation to achieve fast Z-spectral acquisition, we demonstrated the feasibility of fast quantitative HRMAS CEST Z-spectroscopy. The concept was validated with phantoms, which showed excellent agreement with results obtained from conventional HRMAS MR spectroscopy (MRS). We further utilized the HRMAS Z-spectroscopy for fast *ex vivo* quantification of ischemic injury with rodent brain tissues after ischemic stroke. This method allows rapid and quantitative CEST characterization of biological tissues and shows potential for a host of biomedical applications.

Magnetic resonance (MR) techniques are versatile for determining the chemical properties of compounds, for characterizing biological tissues, and for imaging of the human body and organs. Specifically, MR spectroscopy (MRS) characterizes chemical compositions and metabolic changes in a host of pathologies.[1−3] However, routine MRS is susceptible to the signal overlapping due to complex tissue composition, the line shape distortion caused by field inhomogeneity, and the sensible signal line broadening resulting from the overall low mobility of the tissue components, which limit metabolite detection and assignments.[4] High-resolution magic angle spinning (HRMAS) MRS can reduce the line broadening due to dipole−dipole interactions and susceptibility differences within the sample and has demonstrated particular usefulness for studying biological tissues.[5−7]

With the typical sensitivity on the order of millimoles, MRS is limited in detecting the generally low concentration of metabolites in biological tissues.[8,9] In addition, MRS quantification often presents as ratios to a reference metabolite, which may also change under pathological conditions.[9] Recently, chemical exchange saturation transfer magnetic resonance imaging (CEST MRI) has demonstrated its utility

Received: August 11, 2016
Accepted: October 6, 2016
Published: October 6, 2016

ACS Publications © 2016 American Chemical Society

DOI: 10.1021/acs.analchem.6b03137
Anal. Chem. 2016, 88, 10379−10383

for measuring a family of compounds (i.e., proteins/peptides/metabolites) that possess exchangeable protons capable of interacting with bulk water protons.[10] Reported results include studies on creatine,[11,12] glucose,[13,14] and glutamate,[15,16] as well as microenvironment properties such as temperature[17] and pH.[18−21] In brief, exchangeable proton groups in these dilute compounds can be selectively saturated by applying a radiofrequency (rf) pulse at their characteristic frequencies, and the saturated labile proton signal is transferred to the bulk water through chemical exchange, resulting in substantial sensitivity gain for measuring dilute compounds shown in the Z-spectrum.

Z-spectroscopy is often achieved by sweeping rf saturation around the bulk water resonance, offset by offset, which requires prolonged acquisition time[22] (Figure 1a). A fast approach previously developed for studying the magnetization transfer (MT) effect[23] and NMR interactions[24−26] has been adopted recently in CEST Z-spectroscopy.[27,28] This method simultaneously applies rf irradiation and gradient along a direction in which the sample is considered to be homogeneous (Figure 1b). The spectral information is encoded according to their spatial coordinate along the encoding direction. A readout gradient during data acquisition resolves the spatial encoding into CEST spectral frequency. Compared to conventional CEST Z-spectroscopy, which acquires one frequency offset per repetition time (TR), this new approach substantially accelerates the acquisition by collecting all offsets from a single acquisition. The approach has been demonstrated in studies of dia- and para-magnetic CEST agents,[27−29] hyperpolarized Xenon,[30,31] and *in vivo* amide proton transfer (APT) imaging of human white matter.[32] In addition to high-throughput screening of CEST contrast agents, the fast approach has great potential for fast characterization of biological tissues. In this study, to translate Z-spectroscopy to study biological tissues, we combined fast Z-spectroscopy with intact tissue HRMAS MRS, and developed fast tissue HRMAS Z-spectroscopy and quantification.

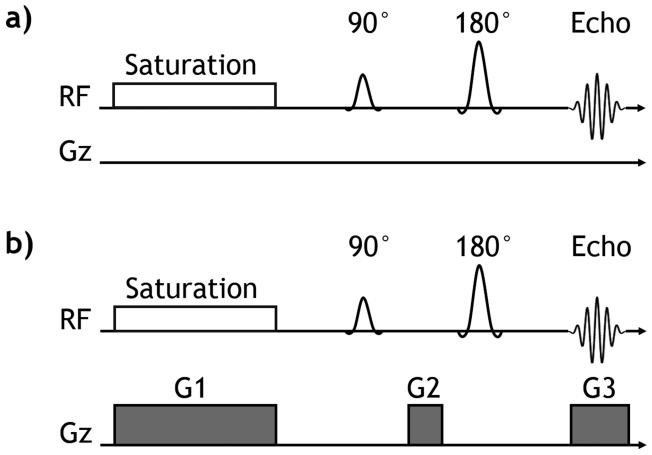

Figure 1. Pulse sequences for (a) routine CEST Z-spectroscopy and (b) fast HRMAS CEST Z-spectroscopy. Routine Z-spectroscopy repeats the saturation experiment per frequency offset. Fast HRMAS CEST spectroscopy utilizes gradient and rf encoding to accelerate the CEST encoding. G1 is a gradient applied during saturation to encode frequency offsets. G2 is a padding gradient applied to the formation of spin echo. G3 is a gradient applied during acquisition.

We first tested the method in a gel phantom containing 30 mM creatine (Cr) on a 14.1 T Bruker AVANCE spectrometer (Bruker BioSpin, Billerica, MA). Spectra were acquired at 4 °C at a spinning rate of 3600 Hz. Instead of FID,[27,28] we collected a spin−echo signal to improve its signal-to-noise ratio. The spectrum acquired without saturation measures the 1D projection of the sample (Figure 2a, top). Z-spectra were derived by normalizing the spectra acquired with rf saturation (B_1 = 1, 1.5, 2, and 3 μT; Figure 2a, middle) to the 1D projection. Z-spectra and corresponding CEST asymmetry (CESTR = $(I_{ref} - I_{label})/I_0$) show strong CEST signal from Cr guanidinium proton at 1.9 ppm relative to bulk water resonance, for different B_1 levels (Figure 2a, bottom). The optimal rf saturation power level was found to be about 1.5 μT (Figure 2b).

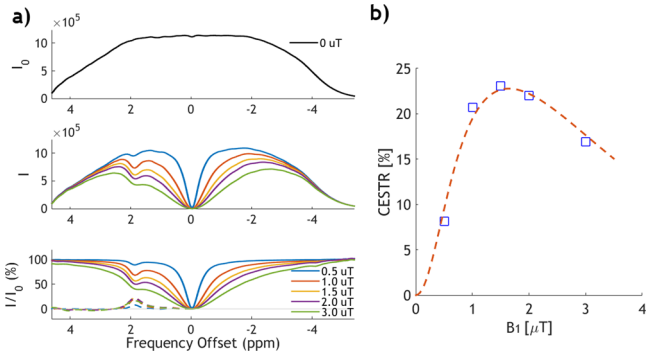

Figure 2. (a) Fast HRMAS CEST Z-spectra from a gel phantom containing 30 mM creatine (Cr) at a spinning rate of 3600 Hz, acquired without (I_0, top) or with (I, middle) saturation pulse at varied power levels. Z-spectra (bottom) were obtained by normalizing I to I_0 and CEST asymmetry (CESTR = $(I_{ref} - I_{label})/I_0$) were shown. (b) CESTR as a function of B_1 level. The optimal B_1 level can be found at 1.5 μT.

We obtained routine HRMAS MR spectra (Figure 3a) and fast HRMAS Z-spectra (Figure 3b, B_1 = 1.5 μT) from a series of gel phantoms containing 10 mM choline (Cho) and varied Cr concentrations of 10, 20, 30, 40, and 50 mM. The two methods revealed major peaks of Cr at 3.0 ppm and at 1.9 ppm, respectively, and the peak increases with Cr concentration. For routine HRMAS MRS, we normalized the integral of Cr peak (3.0 ppm) by that of Cho (3.2 ppm) [Cr/Cho] to generate a relative signal intensity. CESTR at 1.9 ppm was derived for MAS CEST MRS. Figure 3c shows a strong linear correlation between Cr/Cho from conventional HRMAS (R^2 = 0.983, P = 0.001) and CESTR (R^2 = 0.995, P = 0.0001) with Cr concentration, indicating that fast HRMAS Z-spectroscopy is in excellent agreement with routine HRMAS MRS (also see the CEST contrast estimated using Lorentzian decomposition in Figure S1).

We further tested the MAS CEST MRS method with *ex vivo* brain tissue samples from normal reference and ischemic lesion of a rodent stroke model (Figure 4). The Z-spectra show distinct CEST effects at multiple frequency offsets, such as 4.7, 3.5, 2, −2.5, and −3.5 ppm. Importantly, pronounced contrast was observed between the spectra of normal and lesion tissues. Because CEST signal in biological tissues is complicated due to contributions from multiple sources such as amide and amine protons downfield from water,[33] together with semisolid magnetization transfer (MT) asymmetry[34] and aliphatic nuclear Overhauser enhancement (NOE)[35] located predominantly in

DOI: 10.1021/acs.analchem.6b03137
Anal. Chem. 2016, 88, 10379−10383

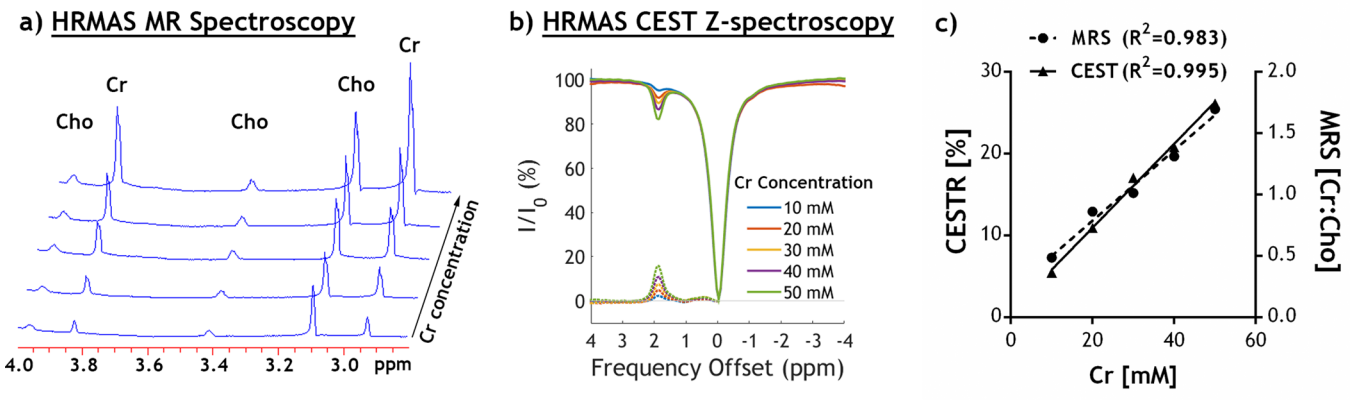

Figure 3. (a) HRMAS MR spectroscopy from gel phantoms containing 10 mM choline (Cho) and different concentrations (10−50 mM) of creatine (Cr) at a spinning rate of 3600 Hz. (b) Z-spectra and CEST asymmetry obtained from the same set of phantoms using the optimal B_1 power of 1.5 μT. (c) Cr level measured as a ratio between Cr and Cho peaks from proton HRMAS spectra and CESTR at 1.9 ppm measured from CEST asymmetry as a function of Cr concentration.

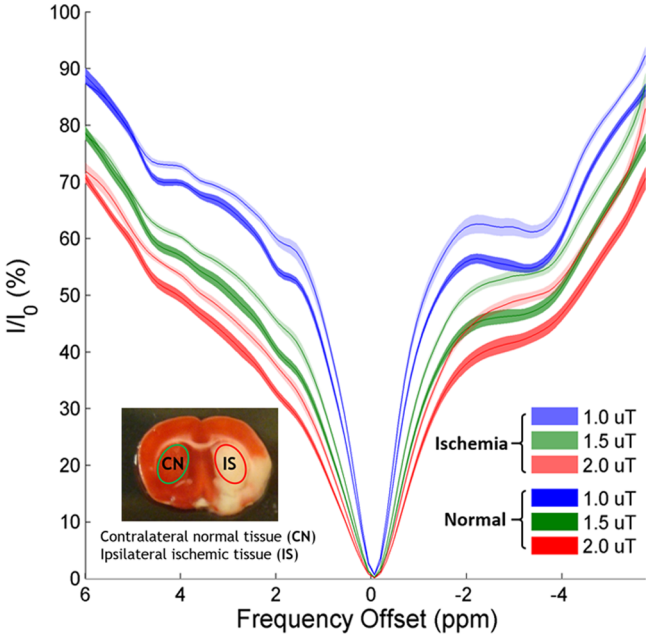

Figure 4. At 24 h after MCAO, brain tissue samples from contralateral normal area or ipsilateral ischemia lesion were harvested and loaded into the rotors. HRMAS Z-spectra of tissue samples from contralateral normal area (dark shaded) or ipsilateral ischemic lesion (light shaded) at 37 °C and a spinning rate of 4800 Hz. Mean ± SEM presented.

the upfield of Z-spectrum, it is critical to identify the CEST effects corresponding to specific solute pools.

Previously, analytical studies confirmed that individual CEST effect and MT effect can be approximated by a Lorentzian line shape in a Z-spectrum if the modeling focuses on the range close to the water peak and the saturation power is relatively low.[22,36,37] Indeed, multiple Lorentzian fitting of the Z-spectrum at low irradiation powers has been increasingly used for quantitative assessment of CEST effects in living tissues.[11,36−40] Here, we fitted the Z-spectrum with a multipool Lorentzian model consisting of direct water saturation (spillover) at 0 ppm, macromolecular MT effect, and multiple CEST pools at 3.5 ppm (amide), 2 ppm (amine), 1 ppm (hydroxyl), and −3.5 ppm (NOE). Because of good spectral resolution at high field, we also included Lorentzian functions centered at 4.7, 2.8, −1.25, and −2.5 ppm, which showed distinguishable CEST effects. Figure 5a shows the multi-Lorentzian decomposition of a representative HRMAS Z-spectrum (B_1= 1 μT) from normal brain tissue (see Figure S2 for distinct CEST peaks after subtracting fitted water and MT from the Z-spectrum). The residuals between the sum of the fitted peaks and the original data were less than 1% (also see

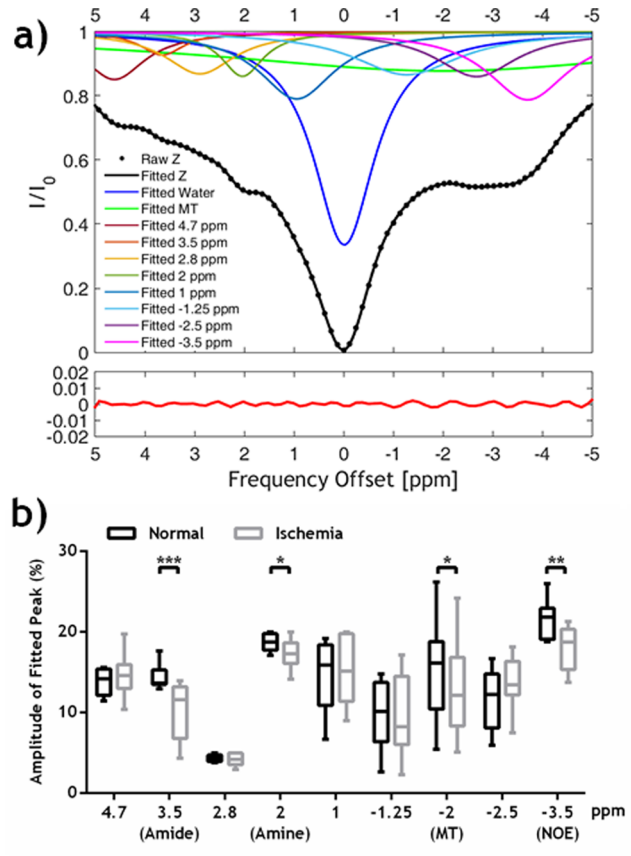

Figure 5. (a) Lorentzian decomposition of a representative HRMAS Z-spectrum (B_1= 1 μT) from normal brain sample. The residuals computed between the sum of the fitted peaks and the original data were shown in the bottom. (b) Boxplot of amplitudes of fitted CEST peaks from normal and ischemic tissue samples (N = 4 animals). Paired Student's t test was performed with *p < 0.05, **p < 0.01, and ***p < 0.005.

DOI: 10.1021/acs.analchem.6b03137
Anal. Chem. 2016, 88, 10379−10383

Figure S3 for fitting quality of HRMAS Z-spectra at the other power levels and ischemic tissue). The goodness of fit (R^2) was above 0.99 for all the Z-spectra. Figure 5b compares the amplitudes of fitted CEST peaks from normal and ischemic tissue samples. Significant differences were found at frequency offsets of 3.5 ppm, 2 ppm, and −3.5 ppm in addition to MT. The CEST effect at 3.5 ppm corresponds to the amide protons, which are often considered from intracellular mobile proteins and peptides and are pH sensitive.[18,20] The reduced CEST effect at 3.5 ppm is likely attributable to acidosis. We also observed decreased CEST effect at 2 ppm, which is associated with amine protons.[37,41] This may be caused by the fact that reduced pH can slow amine proton exchange and make it more visible by CEST MRS.[42,43] We also found significant decreases in the NOE effects in stroke brain, consistent with previous reports.[44] The NOE effects are generally considered to originate from mobile macromolecules, lipids, and restricted metabolites through cross relaxation, which could potentially be exploited as an informative index. The macromolecular MT is slightly asymmetric relative to the water resonance, making it difficult to eliminate using conventional asymmetry analysis.[18,35] Multipool fitting results show noticeable decrease in MT in the ischemic tissue, consistent with findings from MT imaging.[36,45,46] We also observed new CEST effects at multiple other offsets, for example 4.7 ppm and −2.5 ppm, the source of their origins are not clear. This will be explored in the future.

Our study validated the fast quantitative HRMAS CEST Z-spectroscopy in ischemic tissue characterization. Significant changes in the CEST effects of amide, amine protons, as well as the NOE and MT effects were observed. The experimentally measurable CEST effect depends not only on parameters such as labile proton concentration, pH, and temperature but also on relaxation rates. In the ischemic tissue samples, significantly increased longitudinal relaxation time T_1 and transverse relaxation time T_2 were found (Table S1). The T_2 change comes into play through the concomitant rf spillover effect and is accounted for by fitting the direct water saturation in this study. The strong T_1 dependence of CEST effects can be accounted for by normalizing the CEST effect to the measured T_1.[36,47] Indeed, the T_1 correction led to stronger CEST contrasts at the frequency offsets, showing significant changes in ischemic tissue, and revealed significant differences at the offsets of 4.7, 2.8, and 1 ppm that were not detected without correction (Figure S2).

The conventional MRS for biological tissue analysis is highly dependent on the performance of water suppression. HRMAS Z-spectroscopy exploits CEST contrast to investigate the interaction between labile protons and protons in tissue water, and thus no water suppression is required. In addition, the CEST effect is self-normalized to the bulk tissue water and no additional spectral normalization is needed. Compared to conventional Z-spectral acquisition, this fast approach reduces the total acquisition to two scans, equivalent to an acceleration of 64 times (for a Z-spectrum with 128 frequency offsets). Given the Z-spectra acquired using the fast and conventional methods are almost identical,[27,28] we did not collect the conventional Z-spectroscopy. Relatively fast spinning rates were used to avoid potential contamination from spinning sidebands (SSB) in the spectra. Given that the use of low/moderate rotational rates is preferred for biological samples to preserve the structural integrity and to minimize intercompartmental leaks of metabolites, further experiments with optimized sample preparation,[48,49] efficient SSB suppression schemes,[50] and postprocessing methods are needed to obtain SSB-free HRMAS Z-spectrum at slow spinning rates.

In summary, fast tissue characterization using HRMAS CEST Z-spectroscopy can document valuable metabolic information, which augments conventional MRS. In addition, this speedup allows rapid quantification of multipool CEST effects, monitor dynamic changes such as temperature, and high-throughput screening of new CEST contrast agents.

■ ASSOCIATED CONTENT

Supporting Information

The Supporting Information is available free of charge on the ACS Publications website at DOI: 10.1021/acs.analchem.6b03137.

Materials and methods and supplementary data (PDF)

■ AUTHOR INFORMATION

Corresponding Author

*E-mail: pzhesun@mgh.harvard.edu. Phone: (1) 617-726-4060. Fax: (1) 617-726-7422.

Notes

The authors declare no competing financial interest.

■ ACKNOWLEDGMENTS

This study was supported in part by grants from NIH/NINDS Grant 1R21NS085574 (P.Z.S.), NIH/NINDS Grant 1R01NS083654 (P.Z.S.), PHS NIH Grant CA115746 (L.L.C.), and NSFC Grant 81227902 (X. Z.).

■ REFERENCES

(1) Castillo, M.; Kwock, L.; Mukherji, S. K. *AJNR Am. J. Neuroradiol.* **1996**, *17*, 1−15.

(2) Law, M.; Yang, S.; Wang, H.; Babb, J. S.; Johnson, G.; Cha, S.; Knopp, E. A.; Zagzag, D. *AJNR Am. J. Neuroradiol.* **2003**, *24*, 1989−1998.

(3) Duarte, J. M.; Lei, H.; Mlynarik, V.; Gruetter, R. *NeuroImage* **2012**, *61*, 342.

(4) Dong, Z.; Dreher, W.; Leibfritz, D.; Peterson, B. S. *AJNR Am. J. Neuroradiol.* **2009**, *30*, 1096.

(5) Cheng, L. L.; Ma, M. J.; Becerra, L.; Ptak, T.; Tracey, I.; Lackner, A.; Gonzalez, R. G. *Proc. Natl. Acad. Sci. U. S. A.* **1997**, *94*, 6408.

(6) Waters, N. J.; Garrod, S.; Farrant, R. D.; Haselden, J. N.; Connor, S. C.; Connelly, J.; Lindon, J. C.; Holmes, E.; Nicholson, J. K. *Anal. Biochem.* **2000**, *282*, 16.

(7) Sitter, B.; Bathen, T.; Hagen, B.; Arentz, C.; Skjeldestad, F. E.; Gribbestad, I. S. *MAGMA* **2004**, *16*, 174.

(8) Saunders, D. E. *Br. Med. Bull.* **2000**, *56*, 334.

(9) Jansen, J. F.; Backes, W. H.; Nicolay, K.; Kooi, M. E. *Radiology* **2006**, *240*, 318.

(10) Terreno, E.; Castelli, D. D.; Aime, S. *Contrast Media Mol. Imaging* **2010**, *5*, 78.

(11) Cai, K.; Singh, A.; Poptani, H.; Li, W.; Yang, S.; Lu, Y.; Hariharan, H.; Zhou, X. J.; Reddy, R. *NMR Biomed.* **2015**, *28*, 1−8.

(12) Kogan, F.; Haris, M.; Singh, A.; Cai, K.; Debrosse, C.; Nanga, R. P.; Hariharan, H.; Reddy, R. *Magn. Reson. Med.* **2014**, *71*, 164.

(13) Walker-Samuel, S.; Ramasawmy, R.; Torrealdea, F.; Rega, M.; Rajkumar, V.; Johnson, S. P.; Richardson, S.; Goncalves, M.; Parkes, H. G.; Arstad, E.; Thomas, D. L.; Pedley, R. B.; Lythgoe, M. F.; Golay, X. *Nat. Med.* **2013**, *19*, 1067.

(14) Chan, K. W.; McMahon, M. T.; Kato, Y.; Liu, G.; Bulte, J. W.; Bhujwalla, Z. M.; Artemov, D.; van Zijl, P. C. *Magn. Reson. Med.* **2012**, *68*, 1764.

(15) Cai, K.; Haris, M.; Singh, A.; Kogan, F.; Greenberg, J. H.; Hariharan, H.; Detre, J. A.; Reddy, R. *Nat. Med.* **2012**, *18*, 302.

DOI: 10.1021/acs.analchem.6b03137
Anal. Chem. 2016, 88, 10379−10383

(16) Haris, M.; Singh, A.; Mohammed, I.; Ittyerah, R.; Nath, K.; Nanga, R. P.; Debrosse, C.; Kogan, F.; Cai, K.; Poptani, H.; Reddy, D.; Hariharan, H.; Reddy, R. *Sci. Rep.* **2014**, *4*, 6081.
(17) Zhang, S.; Malloy, C. R.; Sherry, A. D. *J. Am. Chem. Soc.* **2005**, *127*, 17572.
(18) Zhou, J.; Payen, J. F.; Wilson, D. A.; Traystman, R. J.; van Zijl, P. C. *Nat. Med.* **2003**, *9*, 1085.
(19) Dorazio, S. J.; Tsitovich, P. B.; Siters, K. E.; Spernyak, J. A.; Morrow, J. R. *J. Am. Chem. Soc.* **2011**, *133*, 14154.
(20) Sun, P. Z.; Wang, E.; Cheung, J. S. *NeuroImage* **2012**, *60*, 1.
(21) Olatunde, A. O.; Dorazio, S. J.; Spernyak, J. A.; Morrow, J. R. *J. Am. Chem. Soc.* **2012**, *134*, 18503.
(22) Zaiss, M.; Bachert, P. *Phys. Med. Biol.* **2013**, *58*, R221.
(23) Swanson, S. D. *J. Magn. Reson.* **1991**, *95*, 615.
(24) Gal, M.; Melian, C.; Demco, D. E.; Blümich, B.; Frydman, L. *Chem. Phys. Lett.* **2008**, *459*, 188.
(25) Andre, M.; Piotto, M.; Caldarelli, S.; Dumez, J. N. *Analyst* **2015**, *140*, 3942.
(26) Frydman, L.; Scherf, T.; Lupulescu, A. *Proc. Natl. Acad. Sci. U. S. A.* **2002**, *99*, 15858.
(27) Xu, X.; Lee, J. S.; Jerschow, A. *Angew. Chem., Int. Ed.* **2013**, *52*, 8281.
(28) Dopfert, J.; Witte, C.; Schroder, L. *J. Magn. Reson.* **2013**, *237*, 34.
(29) Xu, X.; Yadav, N. N.; Song, X.; McMahon, M. T.; Jerschow, A.; van Zijl, P. C.; Xu, J. *J. Magn. Reson.* **2016**, *265*, 224.
(30) Boutin, C.; Leonce, E.; Brotin, T.; Jerschow, A.; Berthault, P. *J. Phys. Chem. Lett.* **2013**, *4*, 4172.
(31) Dopfert, J.; Witte, C.; Schroder, L. *ChemPhysChem* **2014**, *15*, 261.
(32) Liu, Z.; Dimitrov, I. E.; Lenkinski, R. E.; Hajibeigi, A.; Vinogradov, E. *Magn. Reson. Med.* **2016**, *75*, 1875.
(33) Xu, J.; Zaiss, M.; Zu, Z.; Li, H.; Xie, J.; Gochberg, D. F.; Bachert, P.; Gore, J. C. *NMR Biomed.* **2014**, *27*, 406.
(34) Hua, J.; Jones, C. K.; Blakeley, J.; Smith, S. A.; van Zijl, P. C.; Zhou, J. *Magn. Reson. Med.* **2007**, *58*, 786.
(35) Jin, T.; Wang, P.; Zong, X.; Kim, S. G. *Magn. Reson. Med.* **2013**, *69*, 760.
(36) Zaiss, M.; Schmitt, B.; Bachert, P. *J. Magn. Reson.* **2011**, *211*, 149.
(37) Desmond, K. L.; Moosvi, F.; Stanisz, G. J. *Magn. Reson. Med.* **2014**, *71*, 1841.
(38) Jones, C. K.; Huang, A.; Xu, J.; Edden, R. A.; Schar, M.; Hua, J.; Oskolkov, N.; Zaca, D.; Zhou, J.; McMahon, M. T.; Pillai, J. J.; van Zijl, P. C. *NeuroImage* **2013**, *77*, 114.
(39) Zhang, X. Y.; Wang, F.; Jin, T.; Xu, J.; Xie, J.; Gochberg, D. F.; Gore, J. C.; Zu, Z. *Magn. Reson. Med.* **2016**, DOI: 10.1002/mrm.26396.
(40) Windschuh, J.; Zaiss, M.; Meissner, J. E.; Paech, D.; Radbruch, A.; Ladd, M. E.; Bachert, P. *NMR Biomed.* **2015**, *28*, 529.
(41) Jin, T.; Wang, P.; Zong, X.; Kim, S. G. *NeuroImage* **2012**, *59*, 1218.
(42) Mori, S.; Eleff, S. M.; Pilatus, U.; Mori, N.; van Zijl, P. C. *Magn. Reson. Med.* **1998**, *40*, 36.
(43) van Zijl, P. C.; Zhou, J.; Mori, N.; Payen, J. F.; Wilson, D.; Mori, S. *Magn. Reson. Med.* **2003**, *49*, 440.
(44) Li, H.; Zu, Z.; Zaiss, M.; Khan, I. S.; Singer, R. J.; Gochberg, D. F.; Bachert, P.; Gore, J. C.; Xu, J. *NMR Biomed.* **2015**, *28*, 200.
(45) Prager, J. M.; Rosenblum, J. D.; Huddle, D. C.; Diamond, C. K.; Metz, C. E. *AJNR Am. J. Neuroradiol.* **1994**, *15*, 1497−1500.
(46) Kovacs, Z.; Ikezaki, K.; Takahashi, M.; Kawai, J.; Fukui, M. *Acta Neurochir. Suppl.* **1997**, *70*, 43.
(47) Wu, R.; Liu, C.; Liu, P.; Sun, P. Z. *Contrast Media Mol. Imaging* **2012**, *7*, 384.
(48) Renault, M.; Shintu, L.; Piotto, M.; Caldarelli, S. *Sci. Rep.* **2013**, *3*, 3349.
(49) Andre, M.; Dumez, J. N.; Rezig, L.; Shintu, L.; Piotto, M.; Caldarelli, S. *Anal. Chem.* **2014**, *86*, 10749.
(50) Dixon, W. T. *J. Chem. Phys.* **1982**, *77*, 1800.

DOI: 10.1021/acs.analchem.6b03137
Anal. Chem. 2016, 88, 10379−10383